Predicting the Tails of Breakthrough Curves in Regional-scale Alluvial Systems

Yong Zhang and David A. Benson

Department of Geology and Geological Engineering, Colorado School of Mines, Golden, CO 80401

Boris Baeumer

Department of Mathematics and Statistics, University of Otago, Dunedin, New Zealand

Abstract The late tail of the breakthrough curve (BTC) of a conservative tracer in a regional-scale alluvial system is explored using Monte Carlo simulations. The ensemble numerical BTC, for an instantaneous point source injected into the mobile domain, has a heavy late tail transforming from power law to exponential due to a maximum thickness of clayey material. Haggerty et al.'s (2000) multiple-rate mass transfer (MRMT) method is used to predict the numerical late-time BTCs for solutes in the mobile phase. We use a simple analysis of the thicknesses of fine-grained units noted in boring logs to construct the memory function that describes the slow decline of concentrations at very late time. The good fit between the predictions and the numerical results indicate that the late-time BTC can be approximated by a summation of a small number of exponential functions, and its shape depends primarily on the thicknesses and the associated volume fractions of immobile water in "blocks" of fine-grained material. The prediction of the late-time BTC using the MRMT method relies on an estimate of the average advective residence time, t_{ad}. The predictions are not sensitive to estimation errors in t_{ad}, which can be approximated by $L/\bar{v}$, where $\bar{v}$ is the arithmetic mean groundwater velocity and L is the transport distance. This is the first example of deriving an analytical MRMT model from measured hydrofacies properties to predict the late-time BTC. The parsimonious model directly and quantitatively relates the observable subsurface heterogeneity to nonlocal transport parameters.

***Key words**:* Solute transport (Physical processes), Stochastic modeling (Monte Carlo methods), Analytical modeling (Solute transport), Anomalous dispersion, Multi-rate mass transfer, Breakthrough curve

Introduction

The dispersion of conservative solutes in natural porous media is often observed to be "anomalous," which typically denotes non-Gaussian plume shapes and/or non-Fickian growth rates. Either phenomenon may lead to earlier and later arrival of solute at a control plane (i.e., the breakthrough curves (BTCs)), than those predicted for a homogeneous medium. Recent discussions of anomalous laboratory-scale and measured BTCs are given by Benson et al. (2001), Levy and Berkowitz (2003), Bromly and Hinz (2004), and Klise et al. (2004), among many others. Anomalous dispersion can be attributed to the long-range dependence (Dagan 1989) and high variance (Fogg 2004) of the permeability field. Because these two conditions are intrinsic characteristics of typical alluvial systems, a number of detailed studies of anomalous dispersion have been conducted in alluvial aquifers. Generally speaking, the networks of ancient stream channels can form preferential flow paths and cause early arrivals in BTCs, while the surrounding fine-grained aquitard materials sequester the movement of plumes and result in late tails in BTCs (Fogg et al. 2000; LaBolle and Fogg 2001).

Although transport coefficients have been shown numerically to be time-dependent in alluvial systems by LaBolle and Fogg (2001), the quantitative analyses of tailing behaviors of BTCs in regional-scale alluvial systems are still needed, especially for practical problems involving a long time-scale (decades to centuries) and a large space-scale (hundreds to thousands of meters), such as ground water age dating (Weissmann et al. 2002), vulnerability assessment of regional aquifers (Fogg et al. 1998), and evaluation of aquifer remediation by pump and treat techniques (LaBolle and Fogg 2001). Two methods have evolved to simulate the anomalous transport in highly heterogeneous porous media, using either numerical or analytical approaches.

Numerical methods directly simulate aquifer/aquitard structures that might be encountered by a plume. The transport times depend on the architecture of the modeled subsurface heterogeneity, which is commonly built according to various statistical models of observed heterogeneity. In this case, one typically uses the Monte Carlo method to consider a range of equally probable realizations of the heterogeneity. Thus the numerical approach requires the generations of many models, and the repeated computation of water flow and solute transport within these models. Despite of its computational intensity, the Monte Carlo simulation can be the only applicable tool in capturing solute transport for cases where the available, detailed subsurface heterogeneity is critical to solute transport and can not be characterized by any analytical or empirical model. Analytical techniques have been developed to overcome the computational burdens of the numerical approach, but a simple method of developing and parameterizing these equations in a predictive mode (in the absence of tracer tests and/or the Monte Carlo simulations) is lacking.

Several closely related analytical methods have been developed to simulate anomalous dispersion in porous media, especially to capture the heavy tails. Benson et al. (2000) and Schumer et al. (2003) have applied the analytical solutions of non-local, fractional-order advection-dispersion equations (fADE) to predict or fit the skewed and power law early- and/or late-time tails in BTCs. The orders of fractional derivatives characterize the local properties of heterogeneous media. Dentz et al. (2004) have extended the continuous time random walk (CTRW) to reproduce late-time BTCs by assigning a transition density to individual particle motions. The transition densities are due to subsurface heterogeneity, which is analogous to the fADE method. Because they also attempt to capture the transition of later tails from power law to exponential, the transition times used in the CTRW are more general, but require additional fitting parameters. These methods have been applied to fitting the BTCs measured in field or laboratory experiments, in most cases in an empirical manner with limited knowledge of the heterogeneity of the porous medium. The predictive capability of these methods is limited by the unclear quantitative relationship between subsurface heterogeneity and main fitting parameters, which is one of the motivations of this study. Another method proposed by Haggerty and Gorelick (1995) and Haggerty et al. (2000) attempts to capture the later tail of BTCs in mobile domains by accounting for multiple rates of mass transfer between mobile and relatively immobile water. This method has been used for idealized geometries of immobile water, or by fitting BTCs, but it has not been tested in a predictive mode by examining a realistic, complicated hydraulic conductivity (K) distribution. Wang et al. (2005) extended the multirate mass transfer (MRMT) approach of Haggerty et al. (2000) to more general, transient flow fields. They also emphasized the need of tests of the method under realistic field conditions.

The purposes of this study are to 1) explore the tailing behaviors of BTCs for anomalous transport in detailed representations of regional-scale alluvial aquifers; 2) develop applicable analytical or empirical methods to predict the BTCs given the knowledge of heterogeneities; and, 3) explore the influences of geological properties on BTC tails. Based on these analyses, the predictability of the BTC tails can be evaluated systematically, which is important for real-world predictions.

The rest of the paper is organized as follows. First, the Monte Carlo method is used to simulate flow and transport of conservative tracers through an alluvial system based on the data from the Lawrence Livermore National Laboratory site. The numerical BTCs are used as the “real” data for the following prediction and fitting. Second, we extend Haggerty et al.'s (2000) MRMT method to predict the late-time BTC of solutes in the mobile domain, based on the measured thicknesses of low-*K* zones. To our knowledge, this is the first study that attempts to systematically parameterize an analytical MRMT model from measured hydrofacies properties (thicknesses and volume fractions from boring logs) in order to predict the late-time BTCs. Third, the characteristics of the simulated and predicted BTC are discussed in the context of the measured subsurface heterogeneity. Finally, in supplementary material (available as part of the on-line article at http://www.blackwell-synergy.com), we develop a multi-channel transport solution based on the distribution of high-*K* materials to fit/predict the early tail of the BTCs. We also discuss the special difficulties associated with these predictions.

Monte Carlo Calculation of Breakthrough

The transition probability geostatistical approach of Carle and Fogg (1996, 1997) is used to model the spatial variability of aquifer and aquitard units. Their method is based on facies concepts and reduces the reliance on empirical curve-fitting of hydraulic conductivity autocorrelation functions. Readily observable geologic attributes in alluvial settings, including volumetric proportions, mean facies length (e.g., thickness and width), and juxtapositional tendencies (e.g., fining-upward or -downward), can be incorporated directly into development of a three-dimensional transition probability/Markov chain model. The Markov chain model, in turn, is used in a cokriging procedure during conditional sequential indicator simulation and simulated quenching to generate "realizations" of subsurface facies distribution. The mathematical details were given by Carle and Fogg (1996, 1997) and the simulation steps were given by Carle and Fogg (1998). Several interesting applications of this approach are given by Carle et al. (1998). Note that the transition probability/Markov chain model is calculated by the matrix exponential

$$T(h_\phi) = \exp(R_\phi h_\phi) , \tag{1}$$

where T denotes a matrix of interfacies transition probabilities, h_ϕ is a separation vector along direction ϕ, and R is a matrix of transition rates. An eigenvalue analysis showed that the Markov chain model for each entry in $T(h_\phi)$ consists of a linear combination of exponential structures (Weissmann et al. 1999), some of which may have complex rate coefficients indicating cyclicity. Thus the Markov chain potentially may model structures with non-exponentially decaying autocorrelation (Carle and Fogg 1997).

Four hydrofacies: debris flow, floodplain, levee, and channel (Table 1), were identified from detailed interpretations of 5,500m of core taken from an alluvial system at the Lawrence Livermore National Laboratory (LLNL) site (also see LaBolle and Fogg, 2001). The LLNL aquifer system is dominated by fine-grained sediments. The geologic details and the Markov chain model building procedures were discussed by Carle (1996). This Markov chain model has been applied to regional-scale transport models by Fogg et al. (1998) and LaBolle and Fogg (2001). LaBolle at al. (2006) used a similar approach to analyze $^3H/^3He$ fractionation by diffusion and the effect on ground water age dating. In this study, we made two modifications to this model. First, we did not use any of the original conditioning data when generating the facies model, because we wanted to capture the full range of possible spatial variability. Second, we set up a high-*K* zone within each heterogeneity model by assigning “hard” conditioning data consisting of a cluster of high-*K* channel facies in the source area. This high-*K* source area is retained in every aquifer realization and is used as the injection location of contaminants in solute transport modeling. This is done to emphasize the influence of aquifer/aquitard interaction as a plume travels, rather than the influence of the injection facies. To obtain ensemble results, we generated a set of 100 equally probable realizations (one example is shown in Figure 1). Each finite-difference block is 5×10×0.5 m in the depositional strike (x-axis), depositional dip (y-axis), and vertical (z-axis) directions. The overall dimensions of the simulated region are 405×970×40.5 m in each direction, with approximately 640,000 cells in the model domain. The same grid and domain sizes were used in the ground water flow and solute transport simulations described immediately.

The steady-state head and discharge vectors were calculated using MODFLOW (Harbaugh and McDonald 1996). Each cell was given one of four hydraulic conductivity values based on the four simulated hydrofacies determined by the geostatistical realization. The value of each K is equal to the measured average K for each facies. General head boundary conditions were used in the modeling to simulate inflow and outflow through the two lateral boundaries of the model, to minimize the boundary effects on solute transport. Hydraulic head values were defined for the two lateral boundaries using a general gradient of 0.004 parallel to the stratigraphic dip direction (y-axis in Figures 1 and 2). The other boundaries are specified as no-flow conditions (Figure 2).

Solute transport is assumed to follow the classical advection-dispersion equation at the small (local) scale. Transport simulations employed a random walk particle tracking (RWPT) method, described by LaBolle et al. (1996, 1998, 2000, and 2006) and LaBolle (2006). Particles follow analytical streamlines for the advective portion of each motion, and we use an isotropic and constant local-scale dispersivity of 0.01 m and an effective molecular diffusivity of 5.2×10^{-5} m^2/day, which are the same values used by LaBolle and Fogg (2001) in a similar study. The small longitudinal dispersivity was used because previous simulations showed that solute migration is sensitive to the transverse dispersivity, but insensitive to the longitudinal dispersivity, due to the dominant effects of geologic variability as represented in the geostatistical simulations (LaBolle and Fogg 2001). The isotropic dispersivity also optimizes performance of the RWPT algorithm (LaBolle and Fogg 2001; Weissmann et al. 2002). In each Monte Carlo realization, 1,000,000 particles were released at a point at x = 202.5m, y = 855.0m, and z = 19.1m to simulate an instantaneous point source. The injection point is located in the middle of the high-K conditioning cluster (Figure 2). Connectivity analysis (Fogg et al. 2000) indicates that the high-K cluster is always spatially interconnected and fully percolates in the three coordinate directions. Velocity analysis (shown later) demonstrates that the solute transport in the high-K cluster is advection dominated, and thus the source is always placed in a relatively mobile phase within 5×10×2.5 m (the x×y×z size of the high-K cluster) around the injection point. The total modeling time is 10,000 yrs, with a 1-yr interval of output. The control plane extends through the entire domain perpendicular to the main flow direction (Figure 2), and in the following analyses we use L [L] to denote the distance between the point source and the control plane. The simulated BTCs were used as "real" data to test the predictions using the analytical methods described in the next section.

The Analytical MRMT Method to Predict the Late Tail of BTCs

The linear, multiple-rate solute transport equation can be written as follows (Haggerty and Gorelick 1995):

$$\frac{\partial C_m}{\partial t} + \sum_{j=1}^{n} \beta_j \frac{\partial C_{im,j}}{\partial t} = S(C_m), \tag{2}$$

where C_m and $C_{im,j}$ [ML^{-3}] represent the solute concentrations in the mobile zone and the jth immobile zone, respectively, β_j [dimensionless] is the capacity coefficient and is the ratio of contaminant mass in the jth immobile zone to the total mass in the mobile zone at equilibrium, and $S()$ is the linear operator in space representing the advection, dispersion and fluid sources/sinks in the mobile domain. This equation assumes that 1) the contamination is initially placed in the mobile phase (Schumer et al. 2003; Wang et al. 2005), and 2) the porosity does not change with space. Chemical sorption is not modeled in this study. Also note that the classification of immobile zone capacity coefficients in this study depends on the volumes of “blocks” of material with relatively immobile ground water. The rate of mass transfer between C_m and each $C_{im,j}$ can be described by a first-order rate mass transfer model:

$$\frac{\partial C_{im,j}}{\partial t} = \alpha_j \left(C_m - C_{im,j}\right), \tag{3}$$

which has a solution of exponential decay, at rate α_j [T^{-1}], of $C_{im,j}$ for some spike of concentration that is placed in an immobile phase surrounded by clean mobile water.

The summation term in the left-hand side of (2) denotes the change of concentration in immobile zones due to the divergence of advective and dispersive flux of a mobile phase, and it can be expressed as a convolution of the form (Haggerty et al. 2000; Schumer et al. 2003)

$$\sum_{j=1}^{n} \beta_j \frac{\partial C_{im,j}}{\partial t} = g(t) * \frac{\partial C_m}{\partial t}, \tag{4}$$

where the symbol $*$ denotes convolution, and $g(t)$ [T^{-1}] is a “memory function” defined (subsequently) by the proportion of immobile porosity represented by each rate coefficient. By placing (4) into (2), the mobile solute concentration can often be solved when $g(t)$ is known. An approximation of the mobile zone breakthrough at some distance L that is valid for large time is given by Haggerty et al. (2000):

$$C_m(L, t_{late}) \approx t_{ad} \left(C_0\, g - m_0 \frac{\partial g}{\partial t_{late}} \right), \tag{5}$$

where t_{ad} [T] is the average advective residence time of conservative solute in porous media, C_0 [ML^{-3}] is the initial concentration in the mobile phase, and m_0 [MTL^{-3}] is the zeroth temporal moment of the breakthrough curve. For equation (5) to be valid, the observation time t_{late} must be much larger than the sum of the mean advection time across the control plane L and the standard deviation of that advection time (Haggerty et al. 2000). The memory function is a weighted sum of the exponential decay from individual immobile zones (Haggerty et al. 2000):

$$g(t) = \int_0^\infty \alpha b(\alpha) \exp(-\alpha t) d\alpha = \sum_{j=1}^{n} \beta_j \alpha_j \exp(-\alpha_j t), \qquad (6)$$

where $b(\alpha) = \sum \beta_j \delta(\alpha - \alpha_j)$ is a density function of first-order rate coefficients [T]. After inserting (6) into (5), we get the mobile solute concentration at later time after a pulse injection into the mobile zone with zero initial concentration

$$C_m(L, t_{late}) \approx t_{ad}\, m_0 \sum_{j=1}^{n} \beta_j \alpha_j^2 \exp(-\alpha_j t_{late}). \qquad (7)$$

Thus the mobile solute BTC at a control plane at later time is largely dictated by the sum of diffusion times out of all immobile domains between the point of injection and the control plane (see also the discussion in Haggerty et al. 2000).

We will apply equation (7) to predicting the "real" resident concentration of the mobile solute at the later time simulated by the Monte Carlo method. To do this, we first need to define the parameters α_j and β_j in (7). The α_j and β_j were defined to characterize the jth class of immobile zone. Exact expressions for the multirate series of α and β have been proposed and tested by Haggerty and Gorelick (1995) and Haggerty et al. (2000) for various idealized immobile zone geometries including spheres, cylinders and layers. Although their series cannot be used directly in this study due to the irregular geometry and the mixed scales of real-world immobile zones, the general principals can be followed here. Haggerty and Gorelick (1995) defined α_j to be proportional to D^*/R^2, where R [L] is the distance from the center to the edge of the immobile zone. Here we approximate each rate α_j by the inverse of the mean residence time of a particle, which is primarily controlled by the shortest dimension of an immobile block, taken here to be the vertical thickness:

$$\alpha_j = D^* / z_j^2, \tag{8}$$

where z_j [L] is the thickness of the jth class (defined below) of fine-grained sediment. In this study, the immobile block is defined as a cluster composed of floodplain facies in the uniform hydrofacies model. This definition is consistent to the conclusion of LaBolle and Fogg (2001), who find that the diffusion tends to dominate transport in low-permeability floodplain deposits in a similar hydrofacies model. Flow models discussed above also show that the simulated velocities within floodplains are significantly small (with an upper limit around 1×10^{-5} m/day).

The capacity coefficient should be proportional to the ratio of contaminant mass in the immobile zone to the total mass in the mobile zone at equilibrium:

$$\beta_j = \frac{(R_{im})_j (\theta_{im})_j}{R_m \theta_m}, \tag{9}$$

where $(R_{im})_j$ and R_m [dimensionless] are the retardation factors for the immobile zones and the mobile zone, respectively. Here the porosities refer to the ratio of the volume of water in each phase to the total volume of the porous media. In this study, only conservative solutes were considered, and the porosity within each phase is assumed to be constant. Therefore, the porosities in (9) can be converted to the volume fractions of any phase in the aquifer. This simplified β_j, which is proportional to the volume fraction of the immobile block, was then used:

$$\beta_j = f_j \beta_{tot} = \frac{(V_{im})_j}{V_{im}} \beta_{tot}, \tag{10}$$

where $f_j = (V_{im})_j / V_{im}$ [dimensionless] denotes the volume fraction (relative to the volume of the immobile facies) of the jth immobile zone, and $(V_{im})_j$ and V_{im} [L^3] are the volumes of each class of immobile zone and the total immobile facies, respectively. Any number of classification schemes could be used to divide the fine-grained units. Here we define 28 classes up to 14 m thick, in 1/2 m intervals (Figure 3), so that z_j in (8) varies from 0.5 m to 14 m with j from 1 to 28. The immobile zones are classified by their thicknesses, because the immobile blocks with the same thickness have roughly the same mass transfer rate, and the capacity coefficient β_j can be regarded as the weighting function assigned to each associated rate coefficient α_j (Haggerty and Gorelick 1995). The sum of β_j is not 1, but β_{tot}, although in this study, $\beta_{tot}=V_{im}/V_m \approx 1$. This definition is different from Wang et al. (2005), in which $\sum \beta_j = 1$. Note that the parameters for the memory function may be estimated by looking at the geometrical characteristics of the diffusion-limited (low-K) zones. In particular, we use information that may come from the boring logs, because the thicknesses of individual fine-grained units define both the volume proportions and effective rate coefficients. The only unknown parameter in the BTC prediction (7) is the mean advection time t_{ad}. We address this after the next section.

The numerical BTC and the analytical MRMT model developed in this study are limited to conservative tracers. For a reactive tracer with a linear sorption or first-order decay (such as radioactive decay, first-order biodegradation or hydrolysis), the formula (7) with simple modification of transport parameters (as shown by equations (1) and (6) in Haggerty et al. (2000)) or linear decay of mass may still be used to approximate the late-time BTC. Variable retardation and/or porosity in different fine-grained facies can also be easily incorporated into the calculation of β_j in (9). For complex reactions, however, the chemical action term should be added into the governing equation (1) and then transferred into the late-time concentration approximation (7). A non-conservative tracer is beyond the scope of this study, and we leave it for a future study.

Numerical Results

The ensemble BTC from the Monte Carlo simulations are characterized by three primary features:

1) Due to the exponential decay of the transition probabilities, the pdfs of the simulated immobile zone thicknesses are approximately exponential, with a greater number of thin blocks than thick ones (Figure 3). A similar trend is observed in the drillers' logs, although there is more noise in the measured pdf (small rectangles in Figure 3) and higher probability of thicker aquitard layers. The similarity of the simulated and measured pdfs indicates that the aquifer realizations capture most of the statistical properties of the observed heterogeneity (i.e., thickness of clayey materials). Most importantly, it implies the possibility of predicting the late-time solute transport directly from the measured heterogeneity without the burden of explicitly modeling the aquifer heterogeneity, ground water flow, and solute transport.

2) The ensemble numerical BTCs are positively skewed with a steep, Gaussian-like early tail and a heavy late tail (Figure 4). The late-time tail transforms gradually from power-law to exponential at approximately 1,000 years. In our simulations, the slope of the log-log power-law late-time BTC of C_m is always around -2, no matter how distant the control plane is (Figure 4). However, the length of the power law section in BTCs decreases when the control plane distance increases.

3) At later time, the immobile solute BTCs are very close to the total solute BTCs (not shown here), while the mobile solute BTCs have a power law slope 1 steeper than the immobile and total solute BTCs. This differential slope is expected (Schumer et al. 2003) when the memory function has a power law tail.

In all 100 realizations, the velocity at the source cell is $3.6\times10^{-2} \pm 1.7\times10^{-2}$ m/day, which is advection-dominated. Also note that 100 Monte Carlo simulations required 120 hours using SGI Altix 3000 superclusters, with 18 1.3Ghz Itanium2 CPUs and 72 Gigabytes RAM (http://www.aces.dri.edu:8888/sgi-altix.jsp). The same simulations would require months on a personal computer with single CPU. This computational burden motivates our search for simple analytical predictions of ensemble BTC, based on simple measures of the random thicknesses of the relatively mobile and immobile hydrofacies.

Late Tails of Breakthrough Curves

Because we use a control plane at distance L to construct the BTC, we have the ability to calculate several different concentrations at any time. First, we can count the number of random walkers (particles) in the very near vicinity of the plane, regardless of the facies containing the particles. This is denoted $C_{R,total}$: the total resident concentration. We can also distinguish between the mobile facies and immobile facies particles, and we are particularly interested in the mobile resident concentration, denoted $C_{R,m}$. We can further distinguish between particles that have crossed the plane irrevocably, as opposed to particles that have diffused back across the plane, primarily from molecular diffusion but also from the Brownian motion approximation of macrodispersion. Particles that move irrevocably across the plane are counted as the flux, rather than the resident, concentration. The flux concentration may also be present in mobile or immobile facies. The distinction between resident and flux concentration is very important, because the two may differ by orders-of-magnitude, and different field measurement methods will tend toward one or another. For example, a lightly purged monitoring well will measure the resident concentration (also primarily the mobile phase), while a production well measures a flux concentration, because solute particles are removed from the well and cannot move back into the formation. Excellent discussions of the relationship between flux and resident concentrations for classical dispersion are given by Kreft and Zuber (1978) and Toride et al. (1995). Zhang et al. (2006) extended these analyses to some anomalous cases.

Prediction of Late Tails

As discussed above, the only unknown parameter in the BTC late tail prediction (7) is the mean advection time t_{ad}. In a typical alluvial aquifer system, the mean velocity of solutes may be closer to the arithmetic mean velocity (denoted as $\bar{v}$) than other, smaller, mean velocities (such as the geometric or harmonic mean), due to the preferential transport of solutes within paths composed of interconnected high-*K* materials. Solutes also may move much faster than the upscaled (average) pore-water velocity in a heterogeneous porous medium, especially when the medium is dominated by low-permeable sediments. The upscaling of velocity is actually a process of assigning unevenly distributed water fluxes evenly along a cross-section perpendicular to the main flow direction. The solutes, however, usually move preferentially within along sparse but spatially interconnected channels in alluvial systems. Therefore, as a first approximation, the largest mean (arithmetic) of the thickness-weighted average *K* values can be used to estimate $\bar{v}$ and t_{ad}.

To test this hypothesis, we estimated t_{ad} by calculating $\bar{t} = L / \bar{v}$ based on the simulated distributions of hydrofacies. Using this value of $\bar{t}$, along with the memory function $g(t)$ built by equation (6), the prediction is remarkably close to the "real" BTC (Figure 5(b)). Another estimated velocity, the "peak velocity" denoting the local water velocity (which can be measured in the field) at the injection point, is also tested here (Figure 5(a)). Although the *a priori* estimated t_{ad} based on this velocity is about ~3 times smaller than $\bar{t}$, the analytical model still provides a reasonable prediction of late-time BTC (Figure 5(b)). This is because the general trend of the BTCs is not sensitive to the exact value of t_{ad}. Even when the estimation error is one order-of-magnitude higher or lower than the best-fit one (discussed below), the predicted late-time BTC can still capture the general behavior of the "real" late tail of the ensemble BTC.

In the field, we can estimate the upper and lower limits of t_{ad}. Wells in the source area, if present in high-*K* material, can be used as the upper limit of tracer velocities (see the "Peak velocity" in Figure 5(a)). Fluxes at downstream monitoring wells can be calculated too, and the average flux can be used as the approximate value of $\bar{v}$. If one also measures the distribution of the thicknesses of the low-*K* material, then the MRMT method provides a good predictive model of the late-time BTC.

The fitted mean advective residence time, t_{ad}, increases with the increase of distance and asymptotically reaches the time corresponding to $\bar{v}$, the arithmetic mean of ground water velocities in the whole model domain (Figure 5(a)), supporting the use of the simple analytical model. If the control plane distance, *L*, is more than approximately four times longer than the mean length of the channels, then a quick approximation of the mean advection time is $t_{ad} = \bar{t} = L / \bar{v}$.

Influence of Immobile Zone Thicknesses on Late Tails

The best-fit BTCs using the multiple-rate mass transfer method match the numerical late-time BTCs of solutes in mobile domain extremely well (Figure 5(c)). The analytical models capture the transition time of the BTC from power law to exponential, if one is allowed to empirically fit the advection time t_{ad}. The immobile blocks with different thicknesses and volume proportions (i.e., pdfs) have different contributions to the ensemble average of BTCs (Figure 5(c)).

The thicknesses and the associated volume fraction density of immobile blocks control the slope and the transition period of the late-time BTCs. Equation (7) and the fitting results (Figure 5(c)) indicate that solute concentrations can be very closely approximated by a summation of exponential functions (i.e., $\mathbf{exp}(-\alpha_j t_{late})$) with specific weights. The exponential functions themselves depend on the size (thickness) of immobile blocks, and the specific weight of each function depends on the probability (or in the case of a single or real-world realization) volume fraction of layers of a certain thickness.

When tracers originating from mobile zones diffuse into a thin immobile layer, they can exit and diffuse back into the mobile zones relatively quickly. Then these tracers may reach the control plane relatively early and form the early part of late-time BTCs. On the contrary, it takes much longer for the tracers to hit the control plane if they enter a much thicker immobile zone. The thick immobile blocks dominate the latest section of the BTCs, especially the period that the tail transfers gradually from power law to exponential. Note that as shown by Figure 5(c), the exponential-part of late tail is not due to the single, thickest immobile block, but a mixture of several thickest immobile blocks. The lateral boundaries of the numerical model reflected particles back into the domain, simulating an infinite, mirrored system. An alternative model might be one where these boundaries are thick aquitards, or porous bedrock so that mass diffuses into and out of these structures. Very often, in numerical studies, these boundaries are aquitards with large vertical extent, so the boundaries may greatly influence the latest BTC. In fact, the transition from power law to exponential is guaranteed by the finite numerical domain size. Thus a typical field site may have an effectively (with respect to the duration of interest) infinite reservoir into which solute may be sequestered, so that the power law always persists.

The volume fractions of immobile blocks classified by thickness control the slope of the power law late-time BTCs. As mentioned before, we get exponential pdfs of immobile block thickness and the associated volume fraction by using an exponential-form Markov chain transition probability, although the exponential-form transition probability is reported to potentially generate nonexponential-looking structures. The constant slope of power law late-tails is the result of the summation of exponential functions with an exponential pdf. However, the slopes of log-log BTCs observed in field and laboratory tests are not limited to –2. A reliable method, whether Monte Carlo or analytic, should be able to capture a wide range of slopes. To address this, we further tested the MRMT method by assuming different pdfs of volume fractions of immobile blocks classified by thickness. It is difficult to accurately judge the functional form of the pdf of immobile block volumes, especially for the largest blocks. However, a power law pdf of immobile block volumes is possible in some systems (and could be used for the histogram in Figure 3), so we explore the BTC that would result. If the immobile block volume fraction for larger blocks is a power law function of its thickness, i.e., $f_j \propto z_j^{-m}$, then the late-time BTCs contain a power law tail of the form (see Appendix in supplementary material):

$$C_m(L, t_{late}) \quad \propto \quad t_{late}^{(-m-3)/2} \tag{11}$$

for $t_{late} << z_n^2 / D^*$ where z_n is the size of the largest class (for example, in this study we have $t_{late} << z_n^2 / D^* \approx 10^4$ yr). Thus the summation of exponential functions with power law weights is itself a power law function for the time $t << z_n^2 / D^*$. The (power-law part) late tail slope $C_{R,m}$ calculated by the MRMT method should not be limited to –2.

Becker and Shapiro (2003) observe a slope of −2 in their tests in fractured granite, and explain it by the presence of a multitude of slow advection channels. In the present case, however, our low-K zones are clearly diffusion-dominated, with $K = 4.32\times10^{-5}$ m/day (Table 1), so we conclude that the slope is coincidental.

Special caution is needed when using the MRMT method for some cases. For example, when the immobile blocks have variable thickness but a constant volume fraction pdf (e.g., $m = 0$ in (11)), then the mobile power law BTC has a slope of –3/2. When immobile blocks are infinite, the –3/2 slope will last forever. When the immobile blocks have similar thickness and the thickness is small enough, then the late tail of BTC for solutes in all domains remains exponential (i.e., the solution reverts to the single rate mobile/immobile equation, see Toride et al. 1995).

We envision two further studies concerning the features of late-time BTCs that would be valuable. First, using different power-law forms of transition probability, we could generate hydrofacies models with power law distributed thicknesses (and the associated volume fractions) to investigate the veracity of the analytical equation (11). Second, the alluvial system in this study is dominated by fine-grained material. It would be instructive to explore the BTCs in a coarse-grain dominated system (e.g., Weissmann et al. 2002).

We note here that the MRMT method has been shown to be functionally equivalent to the CTRW method (Dentz et al. 2004; Schumer et al. 2003). However, all parameters required by the MRMT method have obvious geologic meanings, and thus they are easily calculated, fitted, or even predicted, given the knowledge of subsurface heterogeneity.

Predictability of the Ensemble Average Versus Individual Realizations

Two control planes were selected to illustrate the variability between realizations and the predictability of the ensemble average BTC with the transport distance. The first plane is 20 m from the source (Figure 6(a)). The second is 600 m away from the source, almost 10 times larger than the mean length of all hydrofacies (Figure 6(b)).

The predictability of the ensemble average BTC at later time becomes better with an increase of transport distance (Figure 6). Poor predictability at short distances might be due to the local spatial variations of hydrofacies between realizations. The hydrofacies distributions generated by stationary transition probabilities can be non-stationary at a small scale close to the mean length of hydrofacies. The non-stationarity results in variations of thickness(es) for the thickest immobile block(s) among realizations. The late-time BTC, therefore, may transform from power law to exponential at different periods among realizations (Figure 6(a)). The non-stationary distributions also let different realizations have a different thickness of the thickest channel(s). The slope of early tail and the peak of BTC, therefore, vary among realizations. On the contrary, a relatively good predictability at long distances is due to the stationary distributions of hydrofacies at a scale much larger than the mean length of hydrofacies (Figure 6(b)).

We did further tests to check whether a single realization with non-point source could be used to assess the ensemble BTC without the computational burden. Realization 5 with a point source produces a BTC significantly different from the ensemble BTC, compared to the other four realizations shown in Figure 6. Hence we selected realization 5 as an example to check whether it can assess the ensemble BTC. Ten million particles (containing the same mass) were released on the upstream plane, and the number of particles within each cell in this plane was scaled by the cell's flux. The particles were almost all in high-permeable cells representing the mobile phase, because the flux through floodplain cell is significantly small compared to the flux in mobile cells. The resultant BTC is similar to the ensemble one (see Figure 7), although the BTC from a single realization has a larger mean advective travel time. Therefore, a single realization with non-point source may assess the main behavior of ensemble BTC. The larger mean advective time is probably due to the lack of the conditioning high-*K* cluster for the cells located in the upstream plane. Further simulations with more realizations are needed to validate the above conclusion.

Transformation between the Late-time Flux and Resident Concentrations

The concentration described by (7) is the resident concentration in the mobile phase. In applications where the detection/injection mode(s) is different, the distinction between the resident versus flux concentrations is necessary (c.f., Kim and Feyen 2000). Furthermore, the determination of risk-based cleanup levels might be most interested in the mobile flux concentration, which could be many orders of magnitude less than the resident concentration (Zhang et al. 2006). Because the main focus of this study is to predict the BTC of $C_{R,m}$, we only discuss the transformation briefly.

For a mobile/immobile model with a power-law memory function $g(t) = t^{-\gamma} / \Gamma(1-\gamma)$ (Schumer et al. 2003), the flux concentration can be transformed directly from its resident counterpart (Zhang et al. 2006):

$$C_F(x,t) \approx \frac{x\gamma}{vt - x(1-\gamma)} C_R(x,t) \quad . \tag{12}$$

However, when the memory function is a summation of exponentials like (6), the transformation cannot be derived analytically, except for the single rate transfer model (for example, see the transformation given by Toride et al. 1993; 1995). Thus we explore the transformation numerically here.

Fitting results (represented by the light lines in Figure 4) suggest the following transform formula

$$C_{F,m}(x,t_{late}) = b\frac{x}{t_{late}} C_{R,m}(x,t_{late}) \quad , \tag{13}$$

where $C_{F,m}$ denotes the flux concentration in the mobile phase, and the fitting parameter b $[TL^{-1}]$ is 0.2 yr/m for all control planes. The transformation (13) may be physically interpreted as the actual travel process: it takes a time of t for the solute with mass $C_{R,m}(x,t)$ to reach (actually cross) location x. The magnitude of b may be related to the velocity v and the memory function $g(t)$, and the best-fit parameter b may imply the similarity of the transformation (13) to (12). Because the slope of the log-log power-law late-time BTC of $C_{R,m}$ is approximately −2 (see Figure 4), the index γ in (12) should be approximately 1 (for details, see Zhang et al. 2006; or Schumer et al. 2003). The best-fit value of b, 0.2 yr/m, is actually very close to the ratio of γ/v. So the formula (13) can be regarded as a special case of (12). Future study is needed to test this hypothesis and explore the geological meaning of the parameter b.

Conclusions

1) Monte Carlo simulations show that the transport of conservative tracers in regional-scale alluvial aquifer/aquitard systems is non-Fickian (or anomalous), because the ensemble BTC

contains a heavy late tail and thus deviates significantly from Gaussian plume. The majority of the late tail decays according to a power law with a final transition to exponential decay. The power law decay of the mobile domain BTC is faster than the immobile domain (and the total domain), with a difference of unity between the slopes on a log-log plot. Furthermore, the BTC based on the flux concentration also decays faster than the resident concentration, and the difference in slopes on a log-log plot is also unity.

2) The late-time concentration for solutes in the mobile domain can be approximated by a weighted sum of exponential functions. The shape of the late tail of BTCs depends on the thicknesses and the associated volume proportions of diffusion-limited layers. This information can be gleaned from boring logs.

3) The late tail of BTCs can be predicted quite accurately using the MRMT method, if we can estimate the mean advective residence time t_{ad}, which can be approximated by $L/\bar{v}$, where $\bar{v}$ is the arithmetic mean of ground water velocities. Accurate prediction of the late-time BTC is relatively insensitive to errors in the estimation of t_{ad}.

4) The difference in breakthrough for each realization, signifying the lack of predictability of a single particular field setting, is greatest for the early BTC at close distances (see also the discussion in supplementary material). When the control plane is located a number of mean facies lengths away from the source, all realizations have similar late-time BTC tails.

5) The application of the MRMT method should not be limited to the fine-grain dominated alluvial system discussed by this study. The MRMT method is appropriate for different pdfs of immobile block volumes and can simulate different late tails.

6) This is the first example of parameterizing an analytical MRMT model from measured hydrofacies properties (volume fractions of fine-grained layers from boring logs) to predict the late time BTCs. We anticipate that the extremely parsimonious model developed in this study may also be used to quantitatively relating the subsurface heterogeneity to nonlocal transport parameters, such as the empirical waiting time density used in the CTRW formalism.

Acknowledgment. D.A.B. and Y.Z. were supported by the National Science Foundation (NSF) grants DMS-0139943 and DMS-0417972, and the grant DE-FG02-07ER15841 from the Chemical Sciences, Geosciences, and Biosciences Division, Office of Basic Energy Sciences, Office of Science, U.S. Department of Energy. Any opinions, findings, and conclusions or recommendations expressed in this material are those of the authors and do not necessarily reflect the views of NSF or DOE. Y.Z. was also partially supported by Desert Research Institute. We thank Scott James, Eric LaBolle, and one anonymous reviewer for their insightful suggestions that improved this work significantly.

References

Becker, M.W., and A.M. Shapiro. 2003. Interpreting tracer breakthrough tailing from different forced-gradient tracer experiment configurations in fractures bedrock. *Water Resources Research* 39, no. 1: Art. No. 1025, doi:10.1029/2001WR001190.

Benson, D.A., S.W. Wheatcraft, and M.M. Meerschaert. 2000. Application of a fractional advection-dispersion equation. *Water Resources Research* 36, no. 6: 1403–1412.

Benson, D.A., R. Schumer, M.M. Meerschaert, and S.W. Wheatcraft. 2001. Fractional dispersion, Lévy motion, and the MADE tracer tests. *Transport in Porous Media* 42, no. 1–2: 211–240.

Bromly, M., and C. Hinz. 2004. Non-Fickian transport in homogeneous unsaturated repacked sand. *Water Resources Research* 40, no. 7: Art. No. W07402, doi:10.1029/2003WR002579.

Carle, S.F. 1996. *A transition probability-based approach to geostatistical characterization of hydrostratigraphic architecture*. Ph.D. Dissertation, University of California, Davis, 248 p.

Carle, S.F., and G.E. Fogg. 1996. Transition probability-based indicator geostatistics. *Mathematical Geology* 28, no. 4: 453–476.

Carle, S.F., and G.E. Fogg. 1997. Modeling spatial variability with one and multidimensional continuous-lag Markov chains. *Mathematical Geology* 29, no. 7: 891–918.

Carle, S.F., and G.E. Fogg. 1998. *TPMOD: A transition probability/Markov approach to geostatistical modeling and simulation*. University of California, Davis, 76 p.

Carle, S.F., E.M. LaBolle, G.S. Weissmann, D. VanBrocklin, and G.E. Fogg. 1998. Geostatistical simulation of hydrofacies architecture: A transition probability/Markov approach. In *SEPM Concepts in Hydrogeology and Environmental Geology No. 1, Hydrogeologic Models of Sedimentary Aquifers*, eds. G.S. Fraser and J.M. Davis, SEPM (Society for Sedimentary Geology), Tulsa Oklahoma.

Dagan, G. 1989. *Flow and Transport in Porous Formations*. Berlin: Springer-Verlag.

Dentz, M., and B. Berkowitz. 2003. Transport behavior of a passive solute in continuous time random walks and multirate mass transfer. *Water Resources Research* 39, no. 5: 1111, doi:10.1029/2001WR001163.

Dentz, M., A. Cortis, H. Scher, and B. Berkowitz. 2004. Time behavior of solute transport in heterogeneous media: transition from anomalous to normal transport. *Advances in Water Resources* 27, no. 2: 155–173.

Fogg, G.E., C.D. Noyes, and S.F. Carle. 1998. Geologically based model of heterogeneous hydraulic conductivity in an alluvial setting. *Hydrogeology Journal* 6, no. 1: 131–143.

Fogg, G.E., E.M. LaBolle, and G.S. Weissmann. 1998. Groundwater vulnerability assessment: hydrogeologic perspective and example from Salinas Valley, CA, in *Application of GIS, Remote Sensing, Geostatistical and Solute Transport Modeling to the Assessment of Nonpoint Source Pollution in the Vadose Zone*, AGU Monograph Series 108, 45–61.

Fogg, G.E., S.F. Carle, and C. Green. 2000. A connected-network paradigm for the alluvial aquifer system. In *Theory, modeling and Field Investigation in hydrogeology: A Special Volume in Honor of Shlomo P. Neuman's 60th Birthday*, ed. D. Zhang, Geological Society of America Special Publication.

Fogg, G.E. 2004. The hydrofacies approach and why lnK $\sigma < 5$-10 is unlikely. *Eos Trans. AGU,* 85(47), Fall Meet. Suppl., Abstract H13H-01.

Haggerty, R., and S.M. Gorelick. 1995. Multiple-rate mass transfer for modeling diffusion and surface reactions in media with pore-scale heterogeneity. *Water Resources Research* 31, no. 10: 2383–2400.

Haggerty, R., S.A. McKenna, and L.C. Meigs. 2000. On the late-time behavior of tracer test breakthrough curves. *Water Resources Research* 36, no. 12: 3467–3479.

Harbaugh, A.W., and M.G. McDonald. 1996. *User's documentation for MODFLOW-96, an update to the U.S. Geological Survey Modular Finite Difference Ground-Water Flow Model*. U.S. Geological Survey Open File Report, 96–485.

Kim, D.J., and J. Feyen. 2000. Comparison of flux and resident concentrations in macroporous field soils. *Soil Science* 165, no. 8: 616–623.

Klise, K.A., V.C. Tidwell, S.A. McKenna, and M.D. Chapin. 2004. Analysis of permeability controls on transport through laboratory-scale cross-bedded sandstone. *Geological Society of America Abstracts with Programs* 36, no. 5: 573.

Kreft, A., and A. Zuber. 1978. On the physical meaning of the dispersion equation and its solutions for different initial and boundary conditions. *Chemical Engineering Science* 33, no. 11: 1471–1480.

LaBolle, E.M., G.E. Fogg, and A.F.B. Tompson. 1996. Random-walk simulation of transport in heterogeneous porous media: Local mass-conservation problem and implementation methods. *Water Resources Research* 32, no. 3: 583–393.

LaBolle, E.M., J. Quastel, and G.E. Fogg. 1998. Diffusion theory for transport in porous media: Transition-probability densities of diffusion processes corresponding to advection-dispersion equations. *Water Resources Research* 34, no. 7: 1685–1693.

LaBolle, E.M., J. Quastel, G.E. Fogg, and J. Gravner. 2000. Diffusion processes in composite porous media and their numerical integration by random walks: Generalized stochastic differential equations with discontinuous coefficients. *Water Resources Research* 36, no. 3: 651–662.

LaBolle, E.M., and G.E. Fogg. 2001. Role of molecular diffusion in contaminant migration and recovery in an alluvial aquifer system. *Transport in Porous Media* 42, no.1–2: 155–179.

LaBolle, E.M. 2006. *RWHet: Random Walk Particle Model for Simulating Transport in Heterogeneous Permeable Media*, v3.2. User's Manual and Program Documentation, 27 p.

LaBolle, E.M., G.E. Fogg, and J.B. Eweis. 2006. Diffusive fractionation of ^{3}H and ^{3}He and its impact on groundwater age estimates. *Water Resources Research* 42, no. 7: W07202, doi:10.1029/2005WR004756.

Levy, M., and B. Berkowitz. 2003. Measurement and analysis of non-Fickian dispersion in heterogeneous porous media. *Journal of Contaminant Hydrology* 64, no. 3–4: 203–226.

Schumer, R., D.A. Benson, M.M. Meerschaert, and B. Baeumer. 2003. Fractal mobile/immobile solute transport. *Water Resources Research* 39, no. 10: Art. No. 1296, doi:10.1029/2003WR002141.

Toride, N., F.J. Leij, and M.Th. van Genuchten. 1993. A comprehensive set of analytical solutions for nonequilibrium solute transport with first-order decay and zero-order production. *Water Resources Research* 29, no. 7: 2167–2182.

Toride, N., F.J. Leij, and M.Th. van Genuchten. 1995. *The CXTFIT code for estimating transport parameters from laboratory or field tracer experiments*, version 2.0. U.S. Salinity Laboratory, USDA, ARS, Riverside CA, 131 p.

Wang, P.P., C. Zheng, and S.M. Gorelick. 2005. A general approach to advective-dispersive transport with multirate mass transfer. *Advances in Water Resources* 28, no. 1: 33–42.

Weissmann, G.S., S.F. Carle, and G.E. Fogg. 1999. Three-dimensional hydrofacies modeling based on soil surveys and transition probability geostatistics. *Water Resources Research* 35, no. 6: 1761–1770.

Weissmann, G.S., Y. Zhang, E.M. LaBolle, and G.E. Fogg. 2002. Dispersion of groundwater age in alluvial aquifer system. *Water Resources Research* 38, no. 10: Art. No. 1198, doi:10.1029/2001WR000907.

Zhang, Y., B. Baeumer, and D.A. Benson. 2006. The relationship between flux and resident concentrations for anomalous diffusion. *Geophysical Research Letters* 33, no. 18: L18407, doi:10.1029/2006GL027251.

Figure 1. A three-dimensional view of the heterogeneous model for Monte Carlo realization 1.

Figure 2. Schematic of flow system. "GHB" denotes the general head boundary. "NFB" denotes the no-flow boundary. L denotes the distance between the point source and the control plane. The main direction of flow is in the depositional dip direction.

Figure 3. Volume fractions of immobile blocks based on their thicknesses: the simulated versus the measured results from the drillers' logs. The dashed line denotes the best-fit power-law trend, with a slope –2.3.

Figure 4. The simulated (symbols) versus the fitted (lines) flux- and resident-concentration based BTCs in the mobile phase (denoted as $C_{R,\,m}$ and $C_{F,\,m}$, respectively) for a control plane located at L = 20m (a), 100m (b), 200m (c), and 400m (d). The dark line denotes the fitted $C_{R,\,m}$ using the MRMT formula (7), and the light line denotes the $C_{F,\,m}$ transformed from $C_{R,\,m}$ using the transformation (13).

Figure 5. (a) The velocity corresponding to the best-fit advective residence time (circles) and some related velocities. "Peak velocity" denotes the local water velocity at the injection point; and "Arithmetic mean velocity" denotes the velocity corresponding to the arithmetic mean of conductivity. (b) The predicted late tails of BTCs using the estimations of t_{ad} for a control plane located at L=100m on a log-log plot. The 21 yr is the (best) predicted t_{ad} based on the arithmetic mean of conductivities. The 8.2 yr represents a prediction based on the "Peak velocity" shown in (a). The 1.8 yr and 180 yr represents an estimation error as high as one order of magnitude of the best-fit t_{ad}. (c) The best-fit late tail of resident concentration based BTC in the mobile phase by

the MRMT method for a control plane located at L = 100m. In the legends, α_1~α_{28} represent the breakthrough associated with each thickness class. The thickness for each α_j is j/2 meter.

Figure 6. The ensemble average of the solute BTCs (dashed line) versus the BTCs of single Monte Carlo realizations (solid lines) for a control plane located at L=20m (a) and L=600m (b), for realizations 1~5 (denoted as R1~R5 in the legend).

Figure 7. The simulated BTC of realization 5 using the single point source (solid gray line) or the multiple source (solid dark line) versus the ensemble average of BTC (dashed line), for the control planes located at L=20 (a) and 100 m (b), respectively. The symbols represent the best-fit concentrations using the MRMT approach (with different mean advective travel times).

Table 1. Hydrofacies properties, including hydrofacies conductivity (m/day), mean length (m), and volumetric proportion.

Hydrofacies	Direction and mean length			Proportion	K (m/day)
	Strike (m)	Dip (m)	Vertical (m)		
Debris Flow	8	24	1.1	7%	0.432
Floodplain	27	67	2.1	56%	0.0000432
Levee	6	20	0.8	19%	0.173
Channel	10	50	1.3	18%	5.184

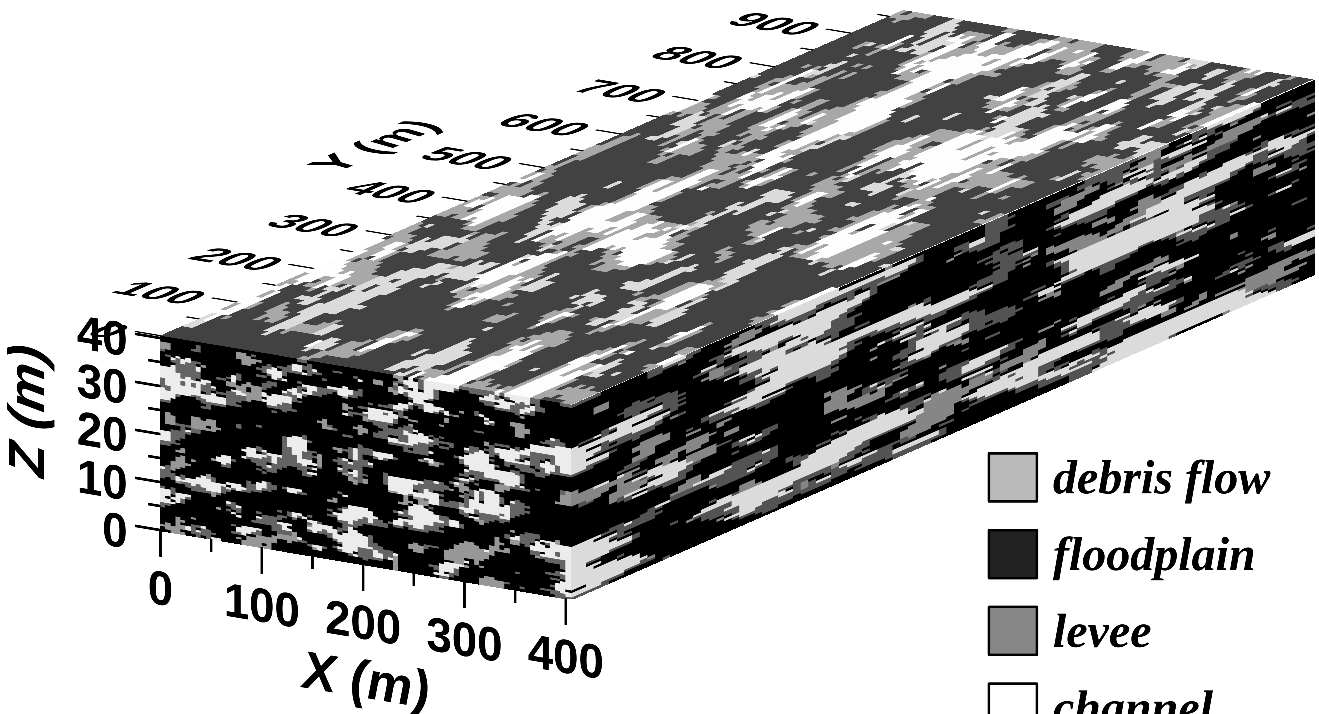

Y (m)
100
200
300
400
500
600
700
800
900
Z (m)
0
10
20
30
40
X (m)
0
100
200
300
400
debris flow
floodplain
levee
channel

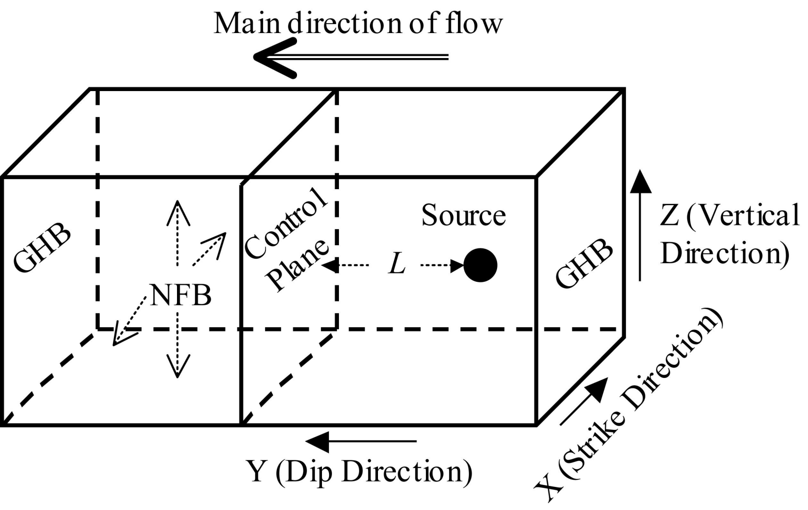

Main direction of flow
GHB
NFB
Control Plane
L
Source
GHB
Z (Vertical Direction)
X (Strike Direction)
Y (Dip Direction)

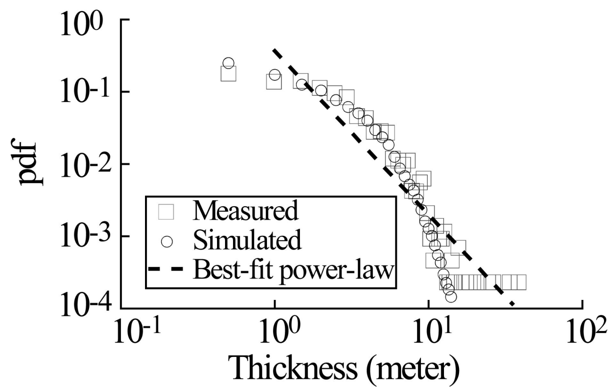

10^0
10^-1
10^-2
10^-3
10^-4
pdf
Measured
Simulated
Best-fit power-law
10^-1
10^0
10^1
10^2
Thickness (meter)

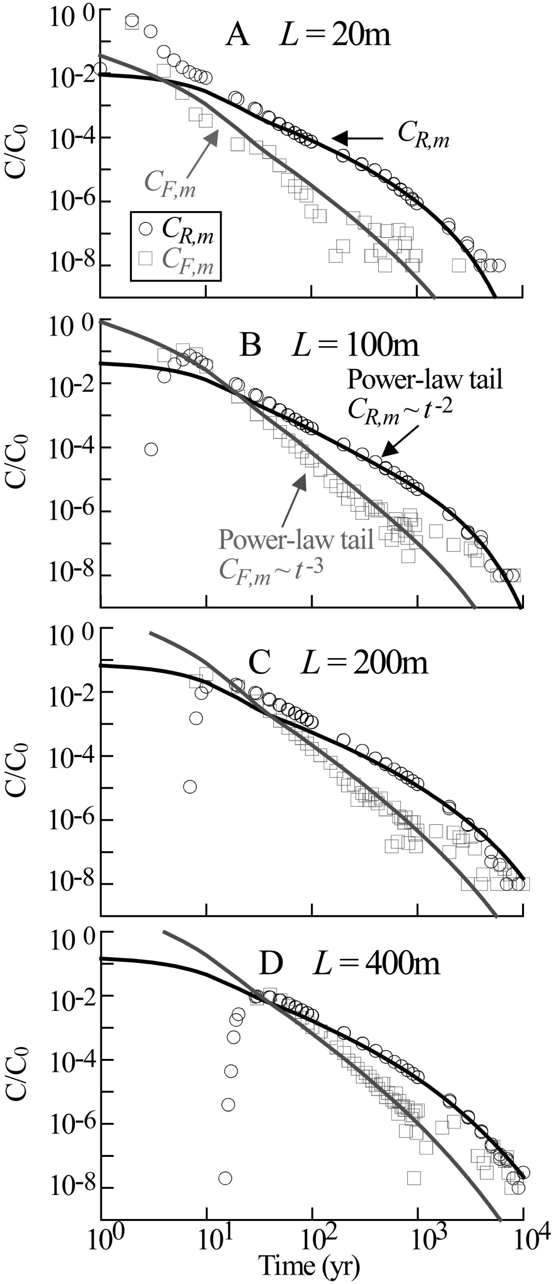

A L = 20m
B L = 100m
C L = 200m
D L = 400m
C/C0
Time (yr)
Power-law tail
C_{R,m} ~ t^{-2}
Power-law tail
C_{F,m} ~ t^{-3}
C_{R,m}
C_{F,m}

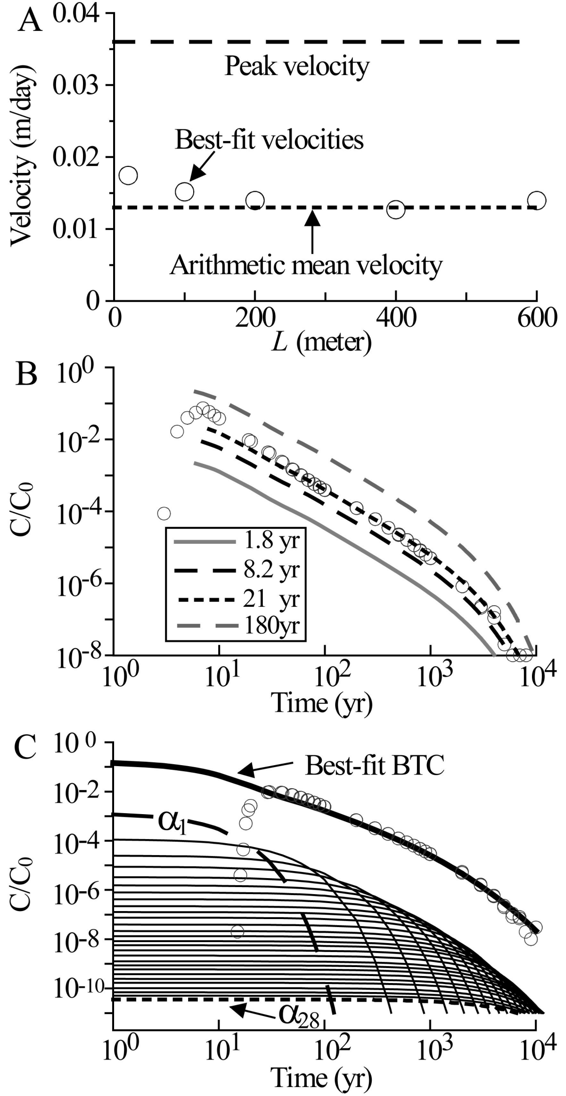

A
Velocity (m/day)
0.04
0.03
0.02
0.01
0
Peak velocity
Best-fit velocities
Arithmetic mean velocity
0
200
400
600
L (meter)
B
C/C0
10^0
10^{-2}
10^{-4}
10^{-6}
10^{-8}
1.8 yr
8.2 yr
21 yr
180yr
10^0
10^1
10^2
10^3
10^4
Time (yr)
C
C/C0
10^0
10^{-2}
10^{-4}
10^{-6}
10^{-8}
10^{-10}
Best-fit BTC
α_1
α_{28}
10^0
10^1
10^2
10^3
10^4
Time (yr)

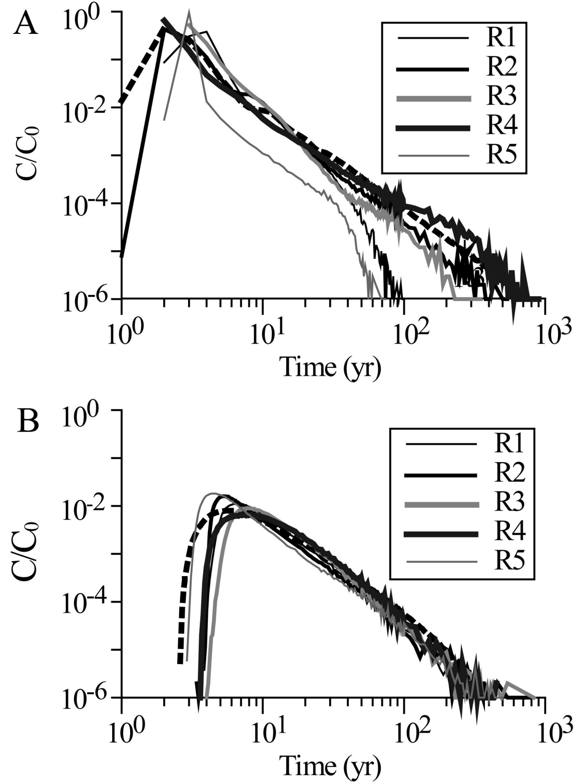

A
B
C/C0
Time (yr)
R1
R2
R3
R4
R5
10^0
10^{-2}
10^{-4}
10^{-6}
10^0
10^1
10^2
10^3

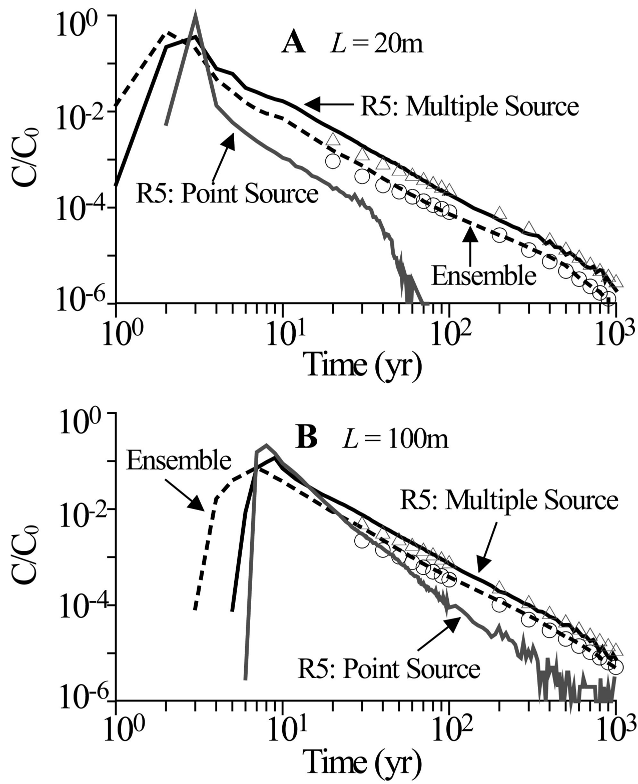

A $L = 20$m
R5: Multiple Source
R5: Point Source
Ensemble
C/C_0
Time (yr)
B $L = 100$m
Ensemble
R5: Multiple Source
R5: Point Source
C/C_0
Time (yr)